ICAS-88-3.2.3

ON MINIMUM TIME TO POINT, MANEUVER, AND SHOOT: SINGULAR PERTURBATION FEEDBACK LAW IN HEAD-ON-PASS ENGAGEMENT*

Dr. Harold Stalford
Eric Hoffman**
Aerospace and Ocean Engineering
Virginia Polytechnic Institute and State University
Blacksburg, Virginia 24060

Abstract

Investigated is the problem of minimizing an airplane's time to point and maneuver against a target in high angle-of-attack flight. Aerodynamic forces and moments are modelled as wind tunnel data. The singular perturbation approach is used to develop nonlinear control for minimizing the time to point, maneuver and shoot in a head-on-pass engagement for the T-2C airplane. The singular perturbation solution is achieved with point, maneuver and point control strategies. The first point strategy snaps the aircraft into an optimal angle-of-attack and pitch rate. The maneuver strategy is nonlinear feedback control that maintains optimal pitch rate and angle-of-attack until target acquisition. The second point strategy achieves equilibrium lock onto target for the shooting mode. The minimum time maneuver strategy is a chattering control. A nonchattering well behaved nonlinear control is derived with very near optimal time response.

1. Introduction

Modern high performance combat aircraft are being designed to provide a new level of dynamic maneuverability called supermaneuverability, Lang and Francis.[1] The performance requirements for such aircraft require high levels of agility and maneuverability at high angles-of-attack (α). The payoff is in the ability to point, maneuver and shoot in minimum time. The concept "point" refers to changing the angle-of-attack while holding the velocity vector fixed. The concept "maneuver" refers to changing the velocity vector while holding the angle-of-attack fixed. In this paper we consider the head-on-pass engagement between the T-2C airplane and a target and we examine the feedback control problem of minimizing the time to point, maneuver and shoot. We investigate the use of singular perturbations, [2] - [9], for deriving nonlinear feedback control to minimize the time.

In this application we simplify the longitudinal model to a constant speed model which reduces the problem to three states and only one control variable. We examine the non-convexity of the hodograph and the chattering control nature of its convex hull. We derive a nonlinear feedback control from the outer layer of singular perturbations. This feedback solution places the optimizing angle of attack at stall, i.e., the peak of the lift curve slope. Feedback controls are also derived for the two transition regions. The first transition solution is a point strategy whereby the angle of attack is brought to its optimizing value, stall. The outer layer nominal feedback control solution is a maneuver strategy whereby the velocity vector is changed appropriately. The second transition solution is a point strategy whereby the airplane locks in equilibrium onto its target for tracking and shooting purposes.

We compare the performance of the singular perturbation feedback solution with that provided by the linear feedback control derived in Stalford and Garrett[10].

2. High Alpha Equations of Motion

We use a longitudinal wind tunnel model of the T-2C airplane, Fortenbaugh[11]. Thrust is removed as a control variable by requiring constant speed V. Consequently, we have only one control δ_e (elevator angle) which we shall denote as δ and three state variables θ (pitch angle), α (angle-of-attack) and q (pitch rate). Under the constant speed assumption, the state equations for zero sideslip are given by Stalford and Garrett[10]

$$\dot{\theta} = q \tag{2-1}$$

$$\dot{\alpha} = q + \frac{1}{\mathrm{Cos}(\alpha)}\left[C_3\,\mathrm{Cos}(\theta) + C_4 C_z(\alpha,\delta) + C_7 C_{z_q}(\alpha) q\right] \tag{2-2}$$

$$\dot{q} = C_1 C_m(\alpha,\delta) + C_6 C_{m_q}(\alpha) q \tag{2-3}$$

$$C_z(\alpha,\delta) = -\left[C_L(\alpha,\delta)\,\mathrm{Cos}(\alpha) + C_D(\alpha,\delta)\,\mathrm{Sin}(\alpha)\right] \tag{2-4}$$

Wind tunnel values of the aerodynamic coefficients C_L, C_D, C_m, C_{z_q} and C_{m_q} are as given in Fortenbaugh[11] and in Stalford and Garrett[10] and are presented in Table A-1 in Appendix A. These functions are plotted in Figure (2-1). Specific numerical values for the T-2C airplane model are presented in Table (2-1) and the evaluation of the constants C_1 - C_7 are given in Table (2-2).

* 16th Congress of the International Council of the Aeronautical Sciences (ICAS), August 28-September 2, 1988, Jerusalem, Israel.

**Also with Ecole Nationale Superieure de l'Aeronautique et de l'Espace, Toulouse, France.

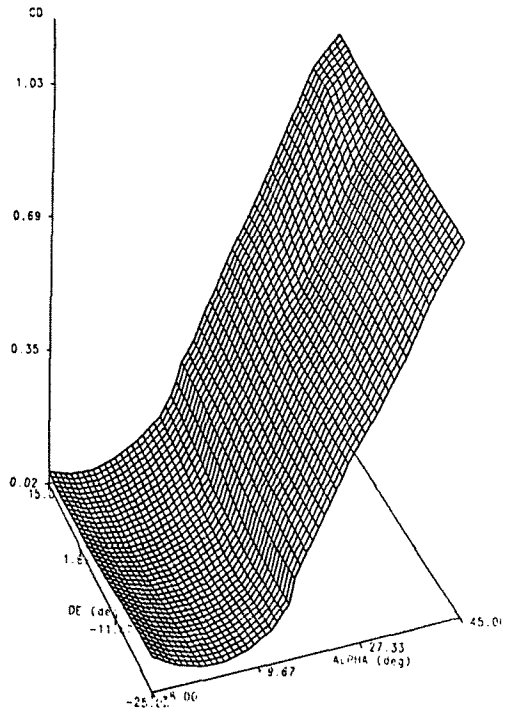

FIG. 2-1a T-2C WIND TUNNEL DATA: DRAG COEFFICIENT FOR ZERO SIDESLIP

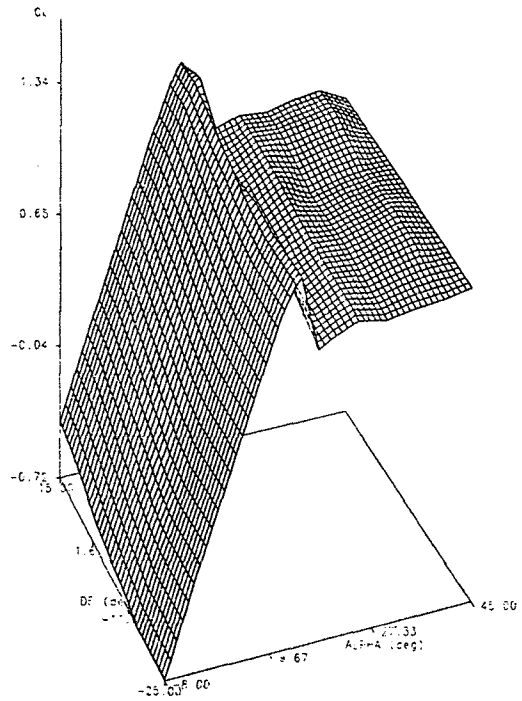

FIG. 2-1b T-2C WIND TUNNEL DATA: LIFT COEFFICIENT FOR ZERO SIDESLIP

Table 2-1. Numerical Values for T-2C Airplane Model

$S = 23.7\ m^2$
$m = 5216.3$ kg
$g = 9.31\ m/sec^2$
$W = mg = 51,171.9$ kg-m/sec^2
$\rho = (1.226)(0.428)$ kg/m^3 (altitude $h \tilde{=} 7500$ m)
$V = 86.297$ m/sec
$I_y = 19.811$ kg-m^2
$\bar{c} = 2.26$ m

Table 2-2. Evaluated Constants for T-2C Airplane Model

$$Q = \frac{1}{2}\rho V^2 = 1953.87 \text{ kg/m-sec}^2$$

$$C_1 = \frac{QS\bar{c}}{I_y} \tilde{=} 5.2826 \text{ 1/sec}$$

$$C_2 = \frac{QS}{W} \tilde{=} 0.9049 \text{ (no units)}$$

$$C_3 = \frac{g}{V} \tilde{=} 0.1137 \text{ 1/sec}$$

$$C_4 = C_2C_3 \tilde{=} 0.1029 \text{ 1/sec}$$

$$C_5 = \frac{\bar{c}}{2V} \tilde{=} 0.0131 \text{ sec}$$

$$C_6 = C_1C_5 \tilde{=} 0.0692 \text{ 1/sec}$$

$$C_7 = C_4C_5 \tilde{=} 0.001347 \text{ (no units)}$$

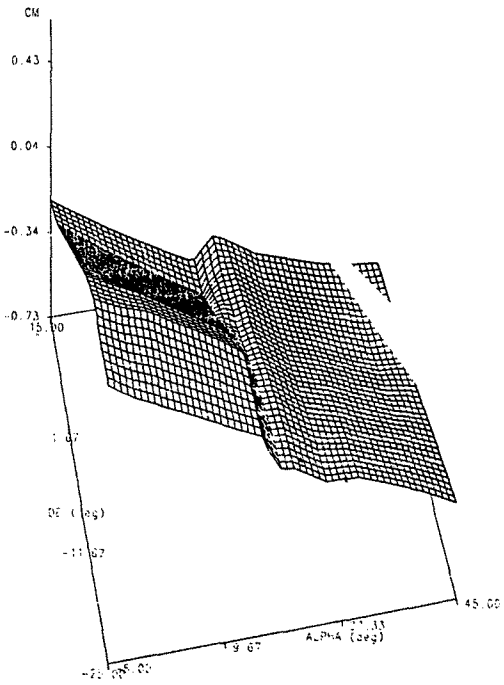

FIG. 2-1c T-2C WIND TUNNEL DATA: PITCHING MOMENT COEFFICIENT FOR ZERO SIDESLIP

3. Minimum Time Performance Index

The objective is to minimize the duration of time to control the T-2C airplane from an initial equilibrium state at time t = 0

$$\theta(o) = \theta_o,\ q(o) = 0,\ \alpha(o) = \alpha_o,\ \delta(o) = \delta_o \qquad (3\text{-}1)$$

to a final reference pitch angle θ_R, zero pitch rate and no condition on the angle-of-attack $\alpha(T)$ at the final time $t_f = T$:

$$\theta(T) = \theta_R,\ q(T) = 0,\ \alpha(T) \text{ and } \delta(T) \text{ are free} \qquad (3\text{-}2)$$

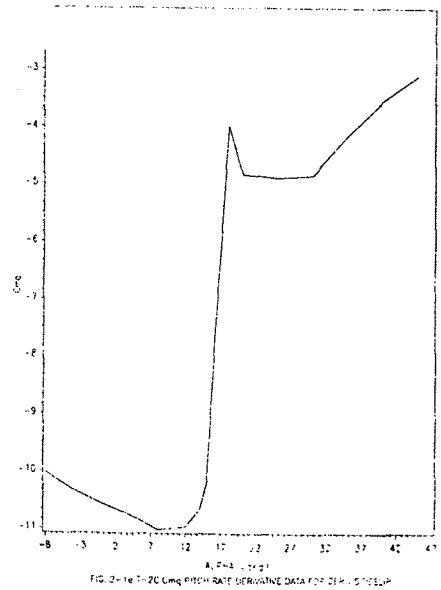

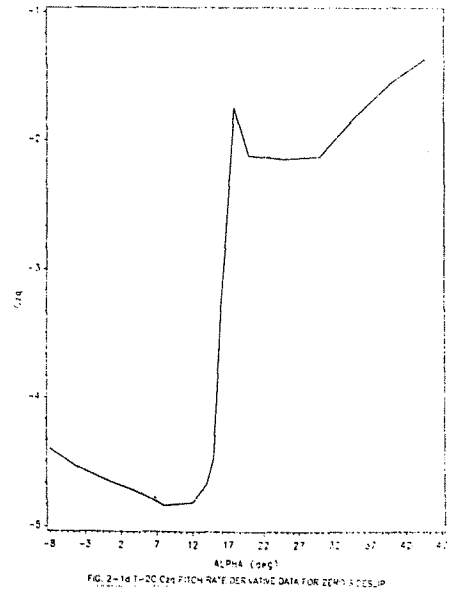

Thus, we are to control the system governed by the state equations (2-1) - (2-3) and render a minimum to the performance index

$$T = \int_0^T dt \qquad (3\text{-}3)$$

In view of Eq. (2-1) this is equivalent to the performance index

$$T = \int_{\theta_0}^{\theta_R} \frac{1}{q}\, d\theta \qquad (3\text{-}4)$$

from which we observe that time is approximately minimized in a singular perturbation outer layer by maximizing pitch rate $q(\theta)$ as a function of pitch angle θ.

4. Non-Convexity of Hodograph

In this section we examine nonchattering and chattering equilibrium points of the $\dot{\alpha}$, $\dot{q}$ equation that maximize pitch rate $q(\theta)$ as a function of pitch angle θ. For fixed pitch angle θ we study $\dot{q}$ and $\dot{\alpha}$ as functions of α, q and δ. We define the domain D in (α,δ) space as those points spanned by $\alpha\varepsilon[-8°,45°]$ and $\delta\varepsilon[-25°,15°]$. For varying levels of q we consider the mapping defined by Eqs. (2-2) and (2-3) from the domain D in (α,δ) space to the image space $(\dot{\alpha},\dot{q})$. We denote that image as $R(q)$. For $\theta = 40°$ Figures (4-1) - (4-4) contain the resulting $R(q)$ for the levels $q = 1.0$, 1.5217, 1.582 and 1.8 deg/sec. We observe that increasing q translates the region $R(q)$ in the positive direction of the $\dot{\alpha}$-axis and nearly parallel to it. In Figure (4-1) the origin $(\dot{\alpha},\dot{q}) = (0,0)$ is contained interior to the image region $R(q = 1.0)$. This origin lies on the boundary of $R(q = 1.5217)$ in Figure (4-2) with $\alpha = 15°$ and $\delta = -11.385$. It lies on the convex hull boundary of $R(q = 1.582)$ in Figure (4-3) with $\alpha = 15°$ and δ chattering between $\delta = -25°$ and $\delta = 10°$. Note that the pitch rate $q = 1.582$ is therefore a chattering solution since the origin lies on the convex hull boundary of $R(1.582)$ but outside $R(1.582)$. The pitch rate $q = 1.5217$ is attainable without chattering at $\alpha = 15°$ with $\delta = -11.385$ since the origin lies on the boundary of $R(1.5217)$. The origin lies outside the convex hull of $R(q = 1.8)$ in Figure (4-4) indicating that the pitch rate $q = 1.8$ deg/sec cannot be sustained as an equilibrium point of the $\dot{\alpha}$, $\dot{q}$ equations at $\theta = 40°$.

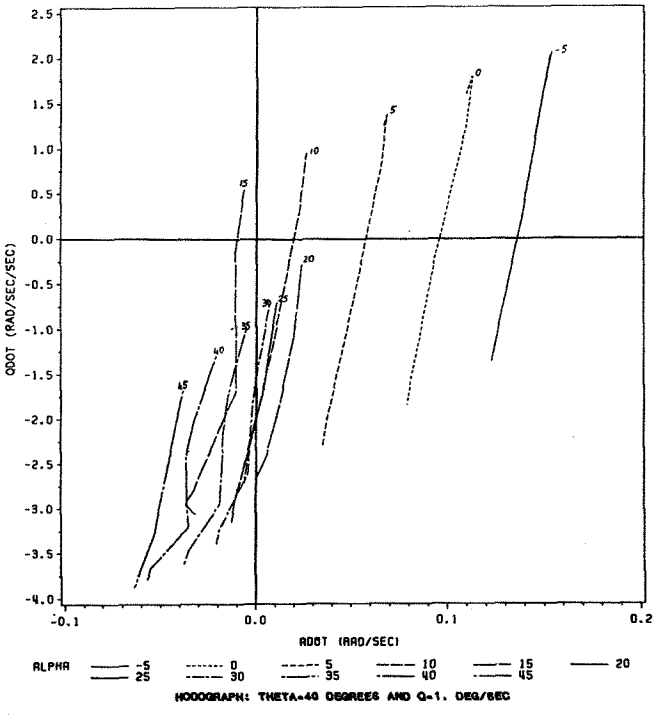

FIGURE 4-1

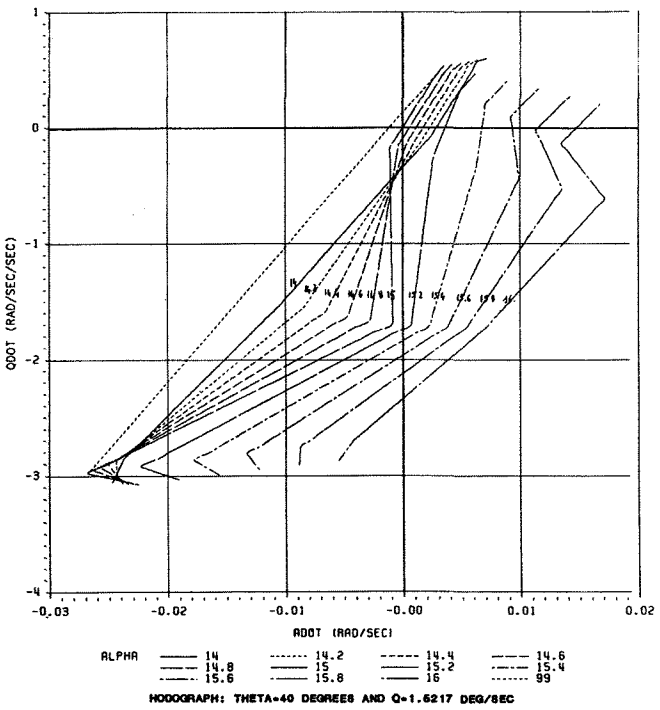

FIGURE 4-2

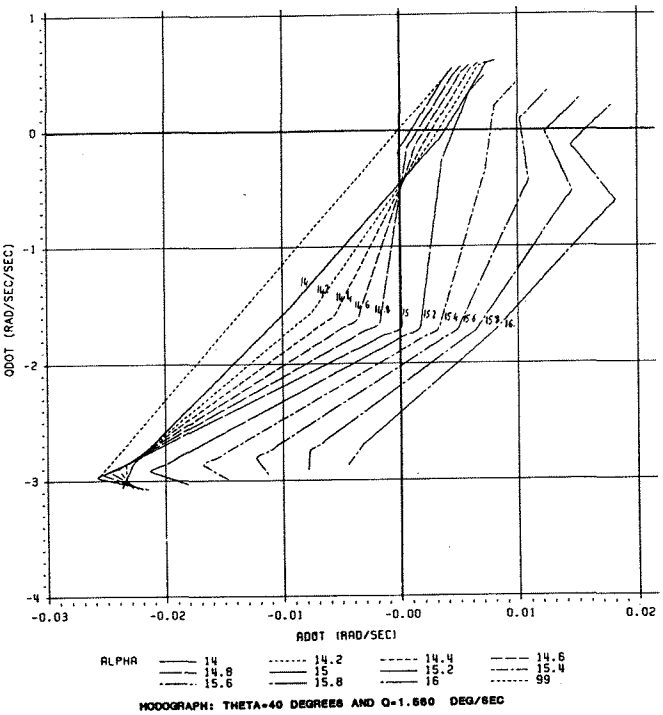

FIGURE 4-3

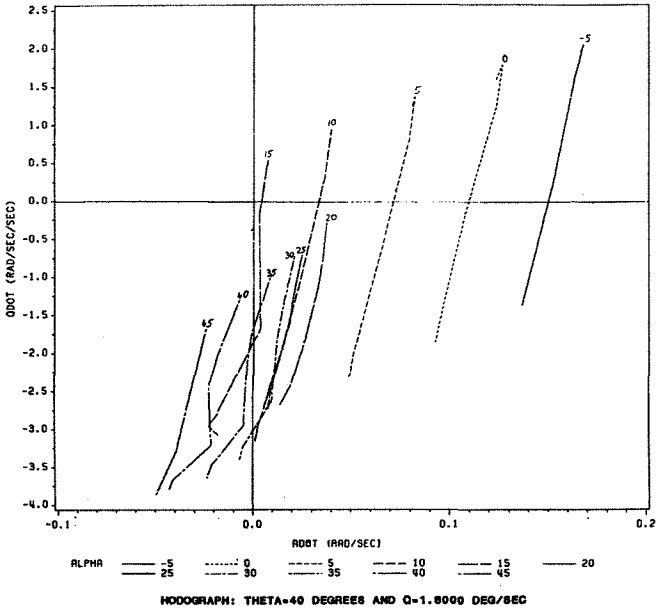

FIGURE 4-4

5. Singular Perturbations: Outer Layer

We assume that α and q are fast variables compared to θ. Consequently, our state equations (2-1) - (2-3) are now:

$$\dot{\theta} = q \tag{5-1}$$

$$0 = q + \frac{1}{\cos(\alpha)} \left[C_3 \cos(\theta) + C_4 C_z(\alpha,\delta) + C_7 C_{z_q}(\alpha) q\right] \tag{5-2}$$

$$0 = C_1 C_m(\alpha,\delta) + C_6 C_{m_q}(\alpha) q \tag{5-3}$$

With our performance index given by (3-4), we minimize the time T by maximizing $q(\theta)$. From (5-2) and (5-3) we have the two analytical expressions of q which is a function of θ, α and δ:

$$q(\theta,\alpha,\delta) = -\frac{1}{\cos(\alpha)} \left[\frac{C_3 \cos(\theta) + C_4 C_z(\alpha,\delta)}{\left[1 + C_7 C_{z_q}(\alpha)\right]}\right] \tag{5-4}$$

$$q(\theta,\alpha,\delta) = -\frac{C_1 C_m(\alpha,\delta)}{C_6 C_{m_q}(\alpha)} \tag{5-5}$$

We maximize q over the domain D of (α,δ) subject to equations (5-4) and (5-5) being satisfied:

$$q^*(\theta) = \max_{\alpha,\delta} \; q(\theta,\alpha,\delta) \tag{5-6}$$

The maximizing arguments of $q(\theta,\alpha,\delta)$ for a given θ are denoted as $\delta^*(\theta)$ and $\alpha^*(\theta)$.

The maximizing argument is independent of θ and is exactly the stall angle of attack:

$$\alpha^*(\theta) = 15° \tag{5-7}$$

This value of α denotes the negative peak of the aerodynamic plunging force coefficient $C_z(\alpha,\delta)$, Figure (5-1). We could have predicted this by considering that (1) δ has only a limited influence on C_z, (2) the quantity $\left[1 + C_7 C_{z_q}(\alpha)\right]$ is near 1.0 and is minimal over the range $\alpha\varepsilon[-8°,15°]$, (3) the quantity $\left[-C_4 C_z(\alpha,\delta)\right]$ is maximum at the stall angle of attack, 15°. Evaluating the constants in (5-4) and using (5-7) we have the approximation

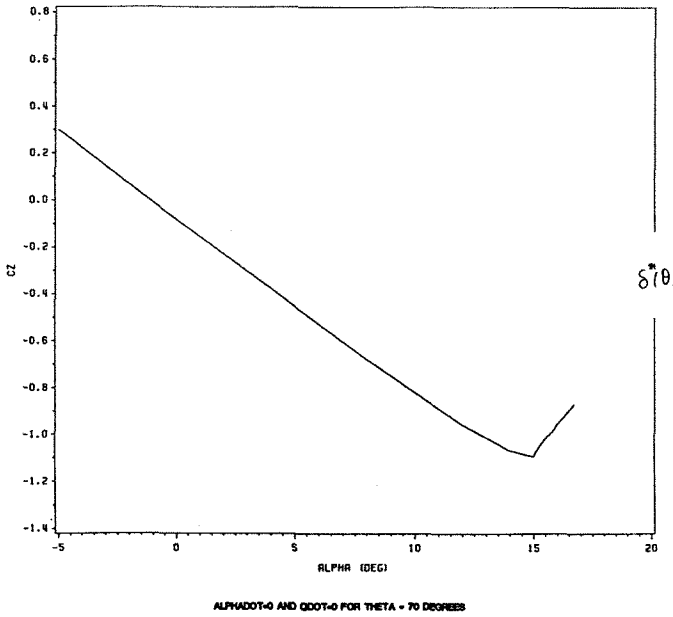

FIGURE 5-1A

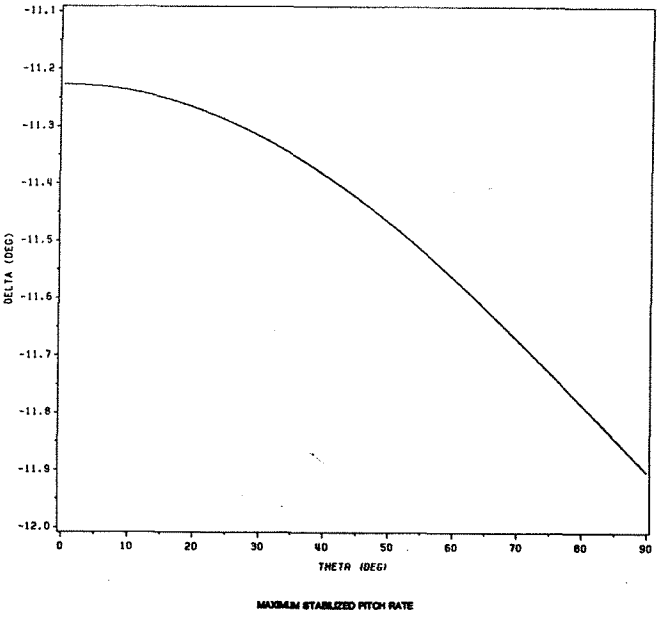

FIGURE 5-2

$$q^*(\theta) = a[1 - \text{Cos}(\theta)] \qquad (5\text{-}8)$$

where a = .118 rad/sec which is about 6.76 deg/sec. Furthermore, if we substitute this approximation into the performance index (3-4) and carry out the integration we obtain the approximation for the minimum time

$$T = -\frac{1}{a}\left[\text{Cotan}\left(\frac{\theta_R}{2}\right) - \text{Cotan}\left(\frac{\theta_o}{2}\right)\right] \qquad (5\text{-}9)$$

The maximizing pitch rate $q^*(\theta)$ is shown in Figure (5-3).

The maximizing argument $\delta^*(\theta)$ is shown in Figure (5-2). The optimal setting varies between -11.9° and -11.2° for all pitch angles θ. We obtain the following approximation by (1) substituting (5-8) into the right-hand side of (5-5), (2) linearizing C_m (15°,δ) using the wind tunnel values and (3) evaluating the constants C_1 and C_6:

$$\delta^*(\theta) = -11.23° - 0.664°[1 - \text{Cos}(\theta)] \qquad (5\text{-}10)$$

Equations (5-8) - (5-10) and Figures (5-2) and (5-3) apply to the nonchattering control, that is, the origin $(\dot{\alpha},\dot{q}) = (0,0)$ lies on the boundary of the hodograph but not on its convex hull, Figure (4-2). As shown in Figure (4-3), an additional pitch rate Δq = .06 degrees/sec can be gained by a chattering control that spends roughly 85% of its time at δ = -25° and the remaining 15% at δ = 10°. In this case the maximizing pitch rate $q_c^*(\theta)$ with chattering control is approximated by

$$q_c^*(\theta) \tilde{=} a(1 - \text{Cos}(\theta)) + b \qquad (5\text{-}11)$$

where a = .118 rad/sec and b = .06/57.3 rad/sec. Therefore, the chattering control reduces the time as given by Eq. (5-9).

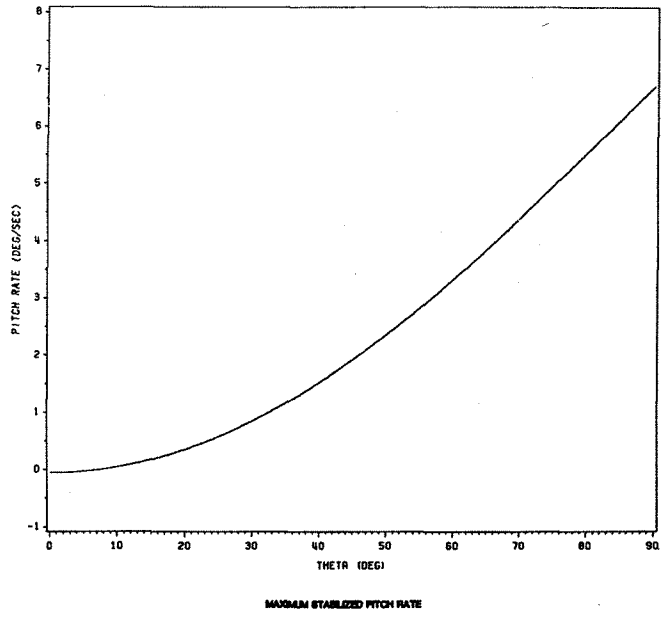

FIGURE 5-3

6. Singular Perturbations: First Inner Layer

Consider θ fixed. We study the transition from (α_o, q_o) to $(\alpha^*(\theta), q^*(\theta))$. We treat α and q as fast variables in this transition. In this first inner layer we assume q is a fast variable as compared to α. From Eqs. (2-2) and (2-3) we have

$$\dot{\alpha} = q + \frac{1}{\text{Cos}\ \alpha}\left[C_3\ \text{Cos}(\theta) + C_4 C_z(\alpha,\delta) + C_7 C_{z_q}(\alpha) q\right] \qquad (6\text{-}1)$$

$$0 = C_1 C_m(\alpha,\delta) + C_6 C_{m_q}(\alpha) q \qquad (6\text{-}2)$$

and from Eq. (3-3)

$$\Delta T_\alpha = \int_{\alpha_o}^{\alpha^*(\theta)} \frac{1}{\dot{\alpha}}\, d\alpha \tag{6-3}$$

To minimize ΔT_α we maximize $\dot{\alpha}$. We seek to determine $\hat{\delta}(\alpha)$ and $\hat{q}(\alpha)$ for each $\alpha\varepsilon[\alpha_o,\alpha^*(\theta)]$ so that Eq. (6-1) is maximized

$$\dot{\alpha}[\hat{\delta}(\alpha),\hat{q}(\alpha)] = \max_{\delta,q} \dot{\alpha}$$

subject to Eq. (6-2) being satisfied and θ held constant. We make the following definitions:

$$a(\alpha) = C_6 C_{m_q}(\alpha) \tag{6-4}$$

$$b(\alpha,\delta) = \frac{C_1 C_m(\alpha,\delta)}{a(\alpha)} \tag{6-5}$$

$$c(\theta,\alpha,\delta) = \frac{C_3\,\mathrm{Cos}(\theta) + C_4 C_z(\alpha,\delta)}{\mathrm{Cos}(\alpha)} \tag{6-6}$$

$$d(\alpha) = 1 + \frac{C_7 C_{z_q}(\alpha)}{\mathrm{Cos}(\alpha)} \tag{6-7}$$

Making use of Eqs. (6-4) - (6-7), substituting q from (6-3) into (6-2) and rearranging terms we have

$$\dot{\alpha}(\theta,\alpha,\delta) = -b(\alpha,\delta)d(\alpha) + c(\theta,\alpha,\delta) \tag{6-8}$$

Numerical results show that Eq. (6-8) is maximized as follows:

Case I: $\alpha_o < \alpha^*(\theta) = 15°$

$$\hat{\delta}(\alpha) = -15° \text{ if } \alpha \leq 13° \tag{6-9a}$$

$$\hat{\delta}(\alpha) = -25° \text{ if } \alpha > 13° \tag{6-9b}$$

Case II: $\alpha_o > \alpha^*(\theta) = 15°$

$$\hat{\delta}(\alpha) = 15° \tag{6-10}$$

The function $\hat{q}(\alpha)$ is determined from Eq. (6-2) using the function $\hat{\delta}$ as defined by Eqs. (6-9) and (6-10):

$$\hat{q}(\alpha) = -b(\alpha,\hat{\delta}(\alpha)) \tag{6-11}$$

7. Singular Perturbation: Second Inner Layer

Consider θ fixed. We continue our study of the transition from (α_o,q_o) to $(\alpha^*(\theta),q^*(\theta))$. The state q is treated in section 6 as being fast as compared to α. Herein, we change q from q_o to $\hat{q}(\alpha)$ assuming that θ and α are fixed. From Eq. (2-3) we have

$$\dot{q} = C_1 C_m(\alpha,\delta) + C_6 C_{m_q}(\alpha) q \tag{7-1}$$

and from Eq. (3-3)

$$\Delta T_q = \int_{q_o}^{\hat{q}(\alpha)} \frac{1}{\dot{q}}\, dq \tag{7-2}$$

we seek maximum $\dot{q}$ for each $q\varepsilon[q_o,\hat{q}(\alpha)]$. We choose $\bar{\delta}(\alpha)$ to maximize $C_m(\alpha,\delta)$. Numerical results reveal:

Case I: $q_o < \hat{q}(\alpha)$

$$\bar{\delta}(\alpha) = -15° \text{ if } \alpha \leq 13° \tag{7-3a}$$

$$\bar{\delta}(\alpha) = -25° \text{ if } \alpha > 13° \tag{7-3b}$$

Case II: $q_o > \hat{q}(\alpha)$

$$\bar{\delta}(\alpha) = 15° \tag{7-4}$$

8. Transition Regions

The hypothesis on multiple time scales cannot be strictly verified especially in the second inner layer. That is, large increases and decreases in $\dot{q}$, as needed at the beginning and at the end of the evolution from θ_o to θ_R, cannot be produced instantly relative to the dynamics of α and θ. Therefore, we study the "switching times" in order to get nearly optimal evolutions of α and θ while being in the outer layer.

The trajectory can be divided into three parts:

(i) transition from (α_o,q_o) to $(\alpha^*(\theta),q^*(\theta))$

(ii) nominal control region of the outer layer

(iii) transition from $q = q^*(\theta_R)$ to $q = 0$.

8.1 End of the first transition

Consider values of the states at the end of the first transition. Assume α is near $\alpha^*(\theta)$ and that the aerodynamic coefficients are almost constants. From Eq. (2-3) we have

$$\dot{q} = a[b(\delta) + q] \tag{8-1}$$

where

$$a = C_6 C_{m_q}(\alpha^*(\theta)) \tag{8-2}$$

$$b(\delta) = \frac{C_1 C_m(\alpha^*(\theta),\delta)}{a} \tag{8-3}$$

Integrating (8-1) from t_o to t_f with $q_o = q(t_o)$, $q_f = q(t_f)$ and $\Delta t = t_f - t_o$

$$q_f = -b(\delta) + e^{a\Delta t}[b(\delta) + q_o] \tag{8-4}$$

Consider the following control law

$$\tilde{\delta}(q) = -25° \text{ if } q < q^*(\theta) \tag{8-5a}$$

$$\tilde{\delta}(q) = 15° \text{ if } q > q^*(\theta) \tag{8-5b}$$

Using Eq. (8-5) we calculate from Eq. (8-4) the time duration Δt needed for q to change from q_o to $q^*(\theta)$:

$$\Delta t = \frac{1}{a} \ell n \left[\frac{q^*(\theta) + b(\tilde{\delta})}{q_o + b(\tilde{\delta})}\right] \tag{8-6}$$

Using (2-2) and (8-6) we compute the evolution induced on α:

$$\dot{\alpha} = [c(\tilde{\delta}) - db(\tilde{\delta})] + d(b(\tilde{\delta}) + q_o)e^{at} \tag{8-7}$$

where

$$c(\tilde{\delta}) = \frac{C_3 \cos(\theta) + C_4 C_z(\alpha^*(\theta), \tilde{\delta})}{\cos(\alpha^*(\theta))} \tag{8-8}$$

$$d = 1 + \frac{C_7 C_{z_q}(\alpha^*(\theta))}{\cos(\alpha^*(\theta))} \tag{8-9}$$

The net change $\Delta\alpha$ in α is

$$\Delta\alpha = [c(\tilde{\delta}) - db(\tilde{\delta})]\Delta t + \frac{d}{a}(b(\tilde{\delta}) + q_o)[e^{a\Delta t} - 1] \tag{8-10}$$

Consequently, in order to bring q to $q^*(\theta)$ at the end of the first transition region we need to apply control law $\tilde{\delta}$ defined by Eq. (8-5) as soon as

$$|\alpha^*(\theta) - \alpha| \leq \Delta\alpha \tag{8-11}$$

8.2 Second and Final Transition Region.

We assume θ is near θ_R. We seek the control law that will bring q to $q_R = 0$ at the same instant that $\theta = \theta_R$. We assume again that the aerodynamic coefficients are constant and that

$$q^*(\theta) > q_R = 0 \tag{8-12}$$

Using Eqs. (2-1) and (8-4) with $\delta = 15°$ we calculate the evolution of θ while $q^*(\theta)$ is changed to $q = 0$:

$$\Delta\theta = -b(\delta)\Delta t + \frac{[b(\delta) + q_o]}{a}[e^{a\Delta t} - 1] \tag{8-13}$$

where

$$\Delta t = -\frac{1}{a} \ell n \left[\frac{q_R + b(\delta)}{q^*(\theta) + b(\delta)}\right] \tag{8-14}$$

as derived in Eq. (8-6) but, in this case, $\delta = 15°$.

Consequently, as soon as

$$\theta_R - \theta \leq \Delta\theta \tag{8-15}$$

we apply the control $\delta = 15°$ in order to get exactly the required θ_R with $q_R = 0$.

9. Feedback Law of Singular Perturbation Analysis

From the singular perturbation analysis of the previous sections we deduce the following feedback law for the transition from $(\theta_o, \alpha_o, q_o)$ to $(\theta_R, \alpha_R, q_R)$ where α_R is free and $q_R = 0$:

(1) First Transition Region, Part I: $\alpha\varepsilon[\alpha_o, \alpha^*(\theta)]$ or $\alpha\varepsilon[\alpha^*(\theta), \alpha_o]$

$q \neq \hat{q}(\alpha)$ and $|\alpha^*(\theta) - \alpha| > \Delta\alpha$

(a) $q < \hat{q}(\alpha)$

$\bar{\delta}(\alpha) = -15°$ if $\alpha \leq 13°$

$\bar{\delta}(\alpha) = -25°$ if $\alpha > 13°$

(b) $q > \hat{q}(\alpha)$

$\bar{\delta}(\alpha) = 15°$

In this initial part of the first transition region we apply control $\bar{\delta}$ to satisfy either $q = \hat{q}(\alpha)$ or $|\alpha^*(\theta) - \alpha| \leq \Delta\alpha$, whichever comes first.

(2) First Transition Region, Part II

$q = \hat{q}(\alpha)$ and $|\alpha^*(\theta) - \alpha| > \Delta\alpha$

(a) $\alpha < \alpha^*(\theta)$

$\hat{\delta}(\alpha) = -15°$ if $\alpha \leq 13°$

$\hat{\delta}(\alpha) = -25°$ if $\alpha > 13°$

(b) $\alpha > \alpha^*(\theta)$

$\hat{\delta}(\alpha) = 15°$

In this second part of the first transition region, we apply control $\hat{\delta}$ until the condition $|\alpha^*(\theta) - \alpha| \leq \Delta\alpha$ is met.

(3) First Transition Region, Part III

$q = \hat{q}(\alpha)$ and $|\alpha^*(\theta) - \alpha| \leq \Delta\alpha$

(a) $\tilde{\delta} = -25°$ if $q < q^*(\theta)$

(b) $\tilde{\delta} = 15°$ if $q > q^*(\theta)$

In this third part of the first transition region we apply control $\tilde{\delta}$ until $\alpha = \alpha^*(\theta)$ and $q = q^*(\theta)$.

(4) Nominal Control Region of Outer Layer

$q = q^*(\theta)$, $\alpha = \alpha^*(\theta)$, $\theta < \theta_R - \Delta\theta_R$

(a) $\delta = \delta^*(\theta)$

In this region of the outer layer we apply control δ^* until θ satisfies $\theta \geq \theta_R - \Delta\theta_R$.

(5) Second Transition Region

$q = q^*(\theta)$, $\alpha = \alpha^*(\theta)$, $\theta \geq \theta_R - \Delta\theta_R$

(a) $\delta = 15°$ until $q = 0$

In this second transition region we apply control $\delta = 15°$ to bring q to zero.

(6) Maintaining $\theta = \theta_R$

$q = 0$

(a) δ is chosen so that $C_m(\alpha,\delta) = 0$.

This final aspect of the feedback control law is to maintain $q = 0$.

10. Simulation Results and Comparison with Linear Feedback Law

We made four simulation runs: one with initial and referenced pitch angles $(\theta_o,\theta_R) = (40°,70°)$, one with $(\theta_o,\theta_R) = (19°,35°)$ and $\alpha_o = 13.4°$, another one with $(\theta_o,\theta_R) = (26.7°,35°)$ and $\alpha_o = 15.8°$ and the fourth one with $(\theta_o,\theta_R) = (10°,35°)$. The four evolutions converged to their assigned θ_R, Figures (10-1) - (10-4). The simulations highlight the importance of the switching time during the transition period to avoid oscillations on α and q that would have led to catastrophic values for the final time. It obliged us to reduce the integration time from 0.05 seconds to 0.0001 seconds around this critical transition region to be sure to switch at the required value of α or θ (over shooting is prevented).

We compare our results with the ones of Stalford and Garrett[10]. In each of the simulations the referenced pitch angle θ_R is reached in shorter time, Figures (4-1a) - (4-4a). Consider the results in Figure 10-1 obtained by the simulation run made with $(\theta_o,\theta_R) = (40°,70°)$ and $\alpha_o = 9°$. The resulting LFB control law and nonchattering singular perturbation (NCSP) control time histories are shown in Figure (10-1c). The LFB control is bang-bang between the control limits -25°, 15°. The NCSP control is better behaved. It is slowly time varying with three brief impulses to handle the transitions to and from the nominal outer layer. In Figure (10-1d) we observe that the LFB α time history oscillates about the stall angle of attack $\alpha = 15°$ while that of the NCSP control is roughly constant during the nominal outer layer.

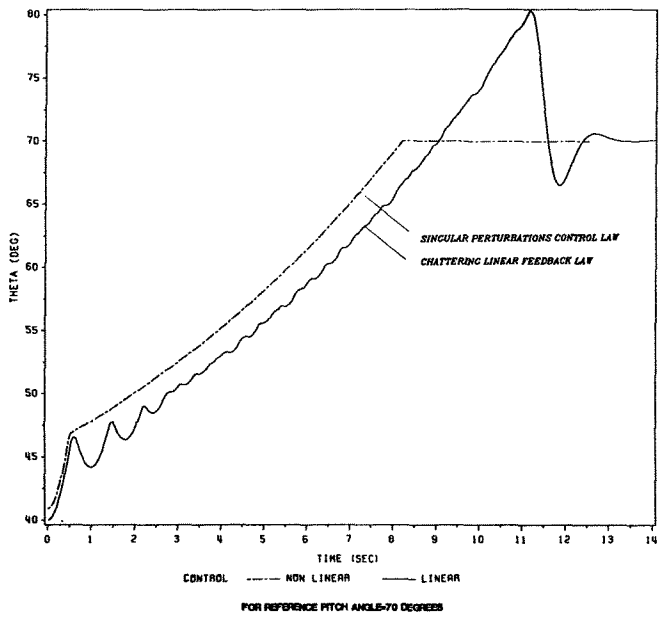

FIGURE 10-1A

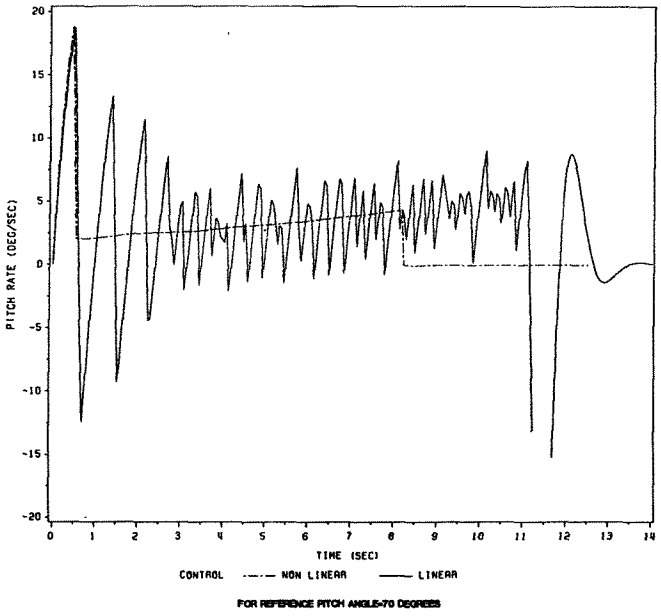

FIGURE 10-1B

We observe in Figure (10-1b) that the pitch rate time history due to the LFB control oscillates whereas that due to the NCSP is roughly constant except at the transition points. The performance of the NCSP control is an improvement over that of the LFB control law. It arrives at the referenced pitch angle θ_R a full second ahead of the corresponding LFB result and there is no over shoot nor nervous behavior during the evolution from θ_o to θ_R as there is in the LFB case. Similar results are obtained for the other simulation runs, Figure (10-2) and (10-3).

The linear feedback (LFB) law is forced into a chattering type control in an attempt to maintain the stall angle of attack $\alpha = 15°$. The root of this chattering phenomenon is observed in Figures (4-2) and (4-3) which shows that the hodograph is non-convex. We understand that the LFB law corresponds to a chattering type solution between $\delta = -25°$ and $\delta = 10°$ or 15° which uses time sharing controls to keep locally $(\dot{\alpha},\dot{q})$ at the origin (0,0). If we permit time sharing between $\delta = -25°$ and $\delta = 15°$ we observe from Figure (4-2) by drawing a straight line between the points $(\dot{\alpha},\dot{q})$ evaluated at $(\alpha,\delta) = (15°,15°)$ and $(\alpha,\delta) = (15°,-25°)$ that this straight line intersects the origin $(\dot{\alpha},\dot{q}) = (0,0)$ at almost the same value of $q = 1.5217$ as the nonchattering singular perturbation solution $\alpha^*(\theta)$, $q^*(\theta)$ and $\delta^*(\theta)$. If we permit time sharing between $\delta = -25°$ and $\delta = 10°$ we observe in Figure (4-3) from the dotted line drawn between the points $(\dot{\alpha},\dot{q})$ evaluated at $(\alpha,\delta) = (15°,10°)$ and $(\alpha,\delta) = (15°, -25°)$ that this straight line intersects the origin $(\dot{\alpha},\dot{q}) = (0,0)$ at the higher value of $q = 1.5817$. Consequently, chattering LFB control between $\delta = -25°$ and 10° will result in improved performance over that achieved by chattering between $\delta = -25°$ and 15°. However, there are differences in performance between a LFB control which chatters between $\delta = -25°$ and 15°, and the nonchattering singular perturbation solution $\alpha^*(\theta)$, $q^*(\theta)$, and

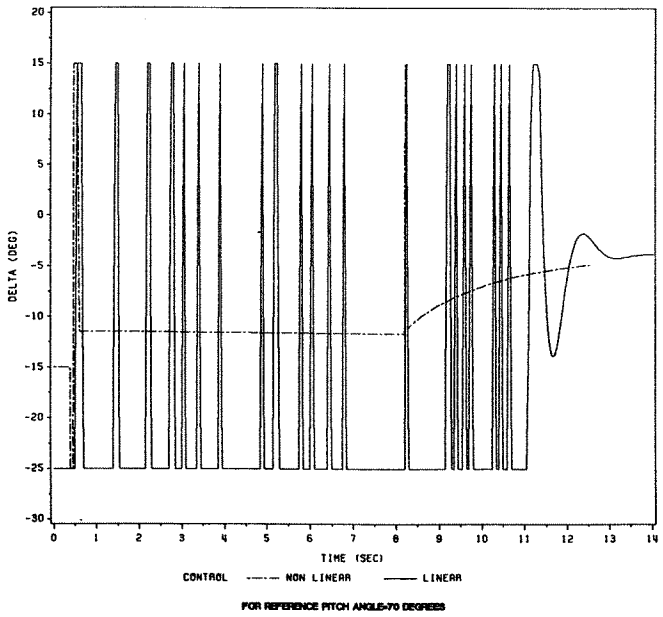

FIGURE 10-1C

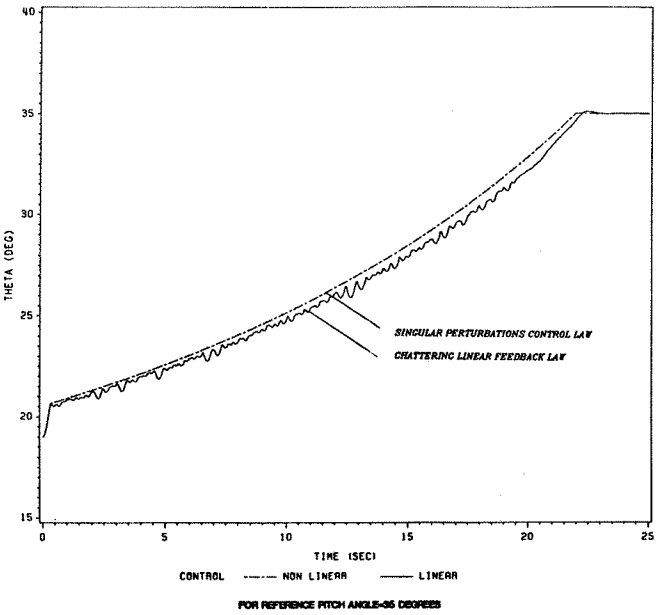

FIGURE 10-2A

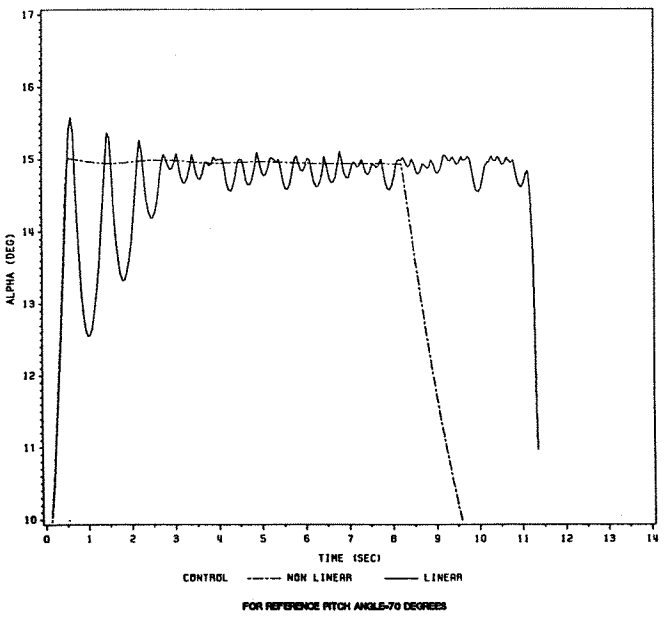

FIGURE 10-1D

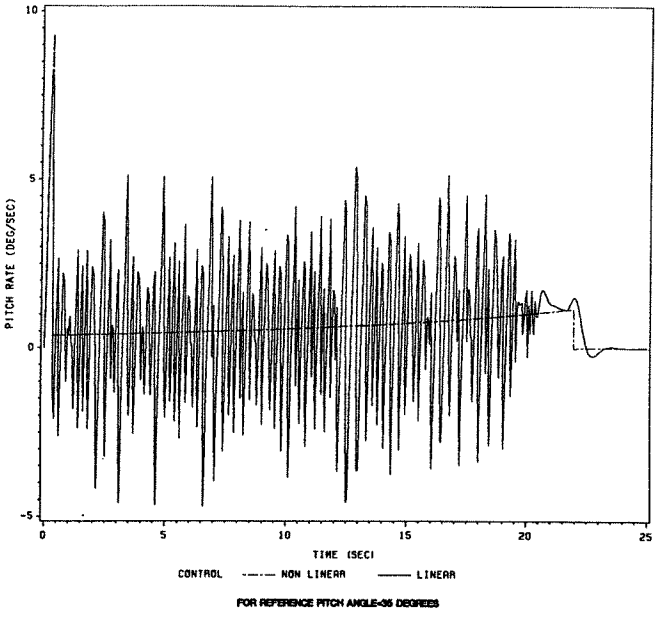

FIGURE 10-2B

$\delta^*(\theta)$ which has the same q-value at the "origin-intersection". This difference in performance is due to the inability of the LFB law to switch infinitely fast between δ = -25° and 15°; here we have assumed a time constant for the elevator actuator of 20 Hertz or an integration time of 0.05 seconds.

We consider the performance of four controls with α_o = 5°, θ_o = 10° and θ_R = 35°.

Control I: A LFB control which "chatters" in a finite fashion at 20 Hertz between δ = -25° and δ = 15°.

Control II: A LFB control which "chatters" in a finite fashion at 20 Hertz between δ = -25° and δ = 10°.

Control III: The nonchattering singular perturbation solution $q^*(\theta)$, $\alpha^*(\theta)$ and $\delta^*(\theta)$.

Control IV: The chattering singular perturbation solution which chatters infinitely fast between δ = -25° and δ = 10°.

The performances of these controls are compared in Figure (10-4). Their performances are in ascending order with Control I corresponding to the bottom curve and Control IV to the top curve. The two lower LFB control performances would approach the upper two singular perturbation solutions as the time constant for the actuator approaches zero.

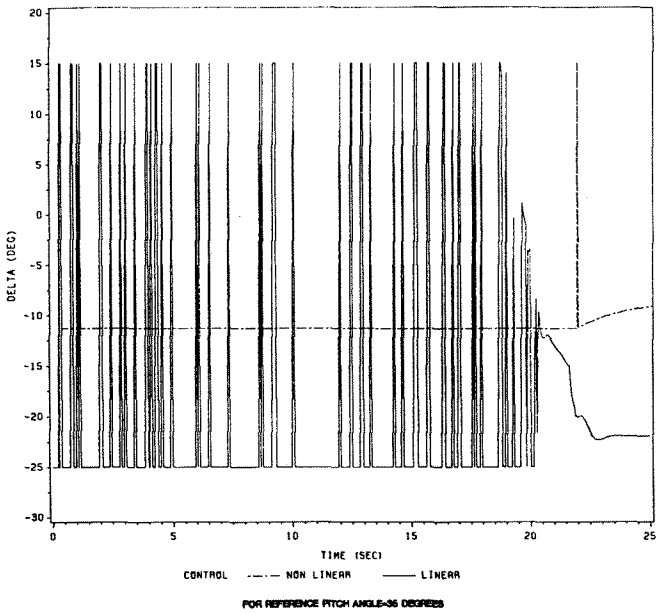

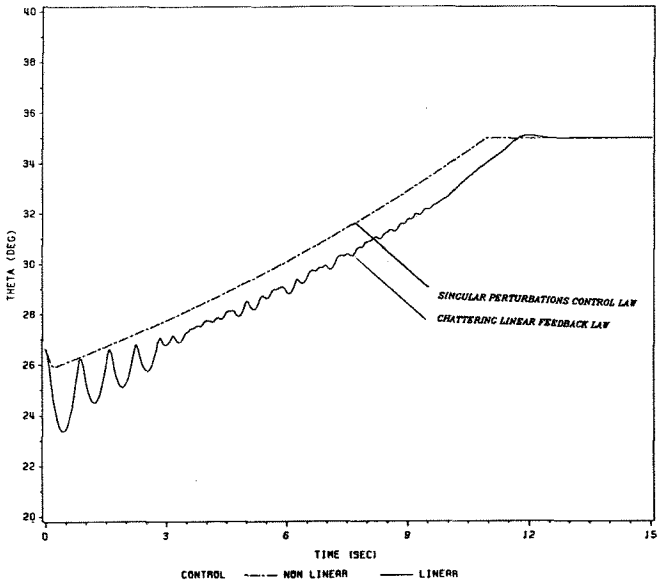

FIGURE 10-3A

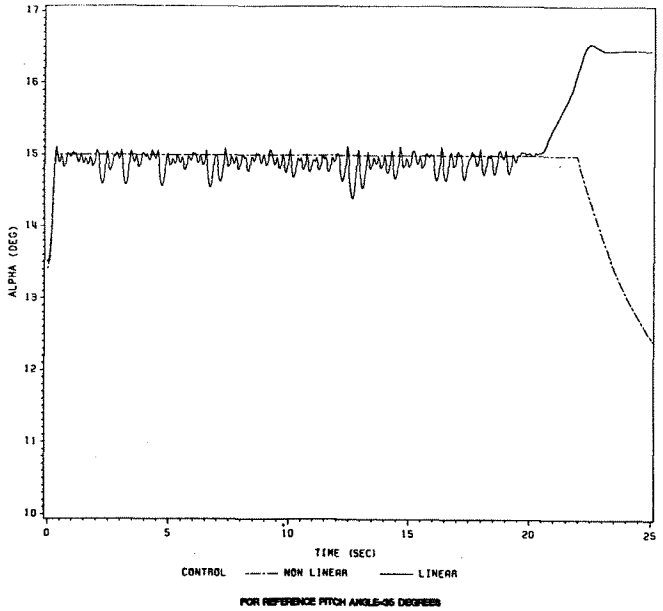

FIGURE 10-2D

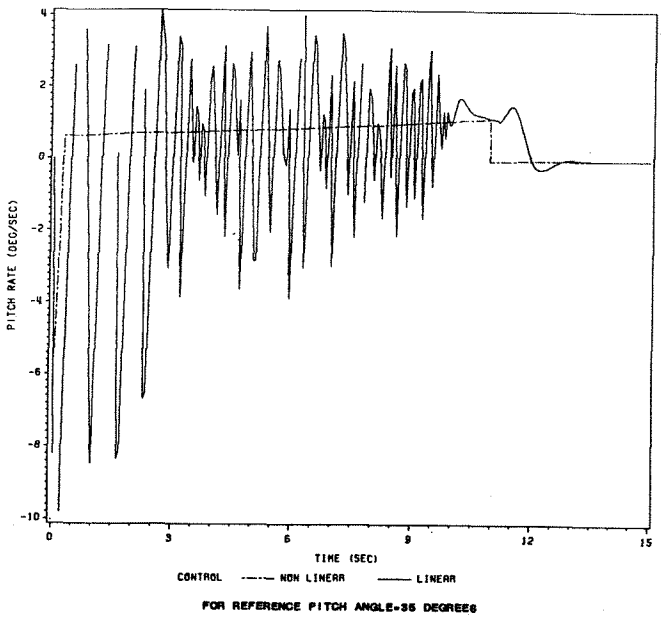

FIGURE 10-3B

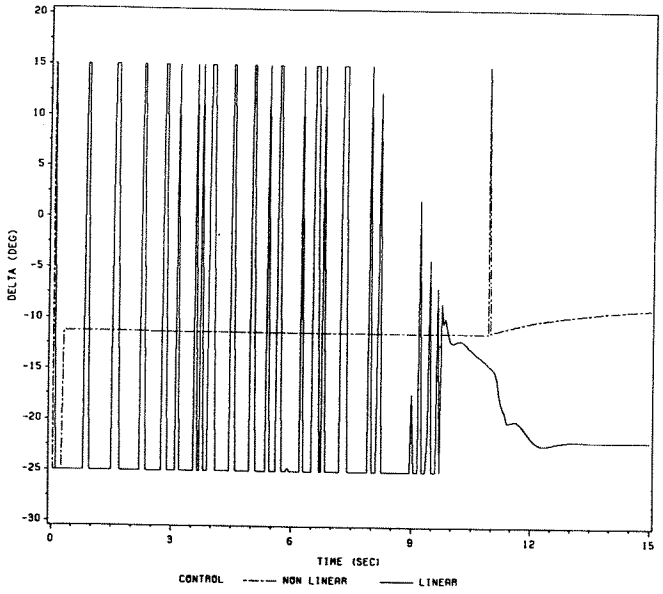

FIGURE 10-3C

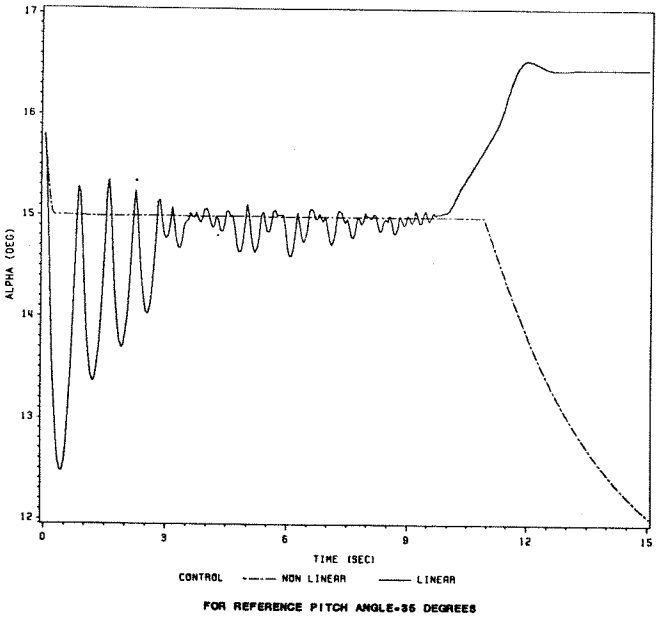

FIGURE 10-3D

11. Comment on Final High α vs. Low α Value

The initial equilibrium values of α (high or low) before the evolution from θ_o to θ_R has no influence on the final value of α after θ_R is reached. It tends toward low alpha equilibrium at infinite time. If we want

$$\theta(t) = \theta_R \text{ for } t \geq T_{final} \qquad (11\text{-}1)$$

Then from $q(t) = 0$ and $\dot{q}(t) = 0$ we have from (2-2) and (2-3)

$$\dot{\alpha} = \frac{1}{\cos \alpha} [C_3 \cos(\theta_R) + C_4 C_z(\alpha,\delta)] \qquad (11\text{-}2)$$

$$0 = C_m(\alpha,\delta) \qquad (11\text{-}3)$$

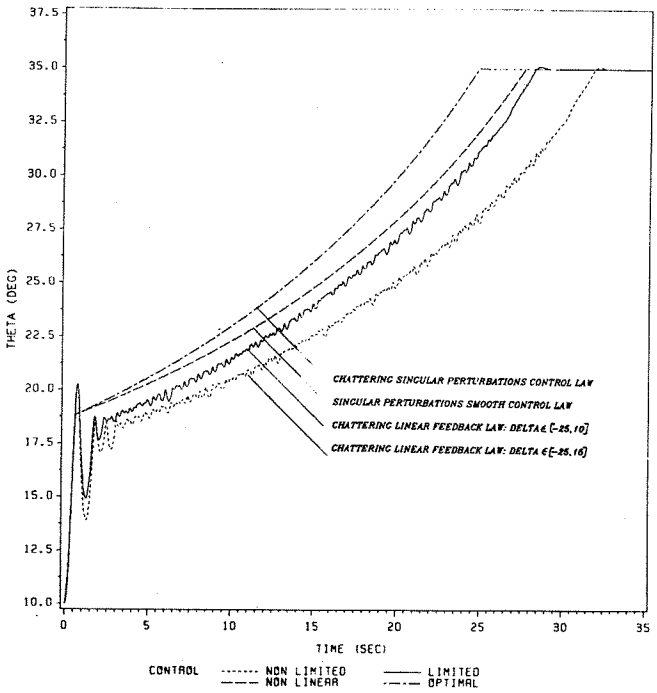

FIGURE 10-4

Consequently, $\dot{\alpha}$ is always negative and it will start to decrease from $\alpha^*(\theta) = 15°$. It will always tend to reach a low alpha equilibrium value. This behavior is observed in Figures (10-1d), (10-2d) and (10-3d).

12. Conclusion

The singular perturbation approach of developing nonlinear control to minimize the time to point, maneuver and shoot in a head-on-pass engagement has revealed several interesting results. First, the singular perturbation feedback control on the outer layer is shown to be chattering (infinitely fast) due to the non-convexity of the hodograph. Second, a realizable nonchattering control which lies on the boundary of the hodograph but not on the boundary of the convex hull is shown to have a performance which is very close to that of the chattering control. Third, the singular perturbation solution for the nominal outer layer places the optimizing angle of attack $\alpha^*(\theta)$ at stall $\alpha = 15°$ with no dependence on the pitch angle. Fourth, the feedback control $\delta^*(\theta)$ along the nominal outer layer varies between the narrow limits -11.9° and -11.2°. Fifth, the nonchattering singular perturbation solution is shown to have superior performance as compared to that of a linear feedback controller which is limited in its behavior to chatter between the two optimal time sharing control settings $\delta = -25°$ and $\delta = 10°$ due to the dynamics of an actuator.

We emphasize that the results contained in this paper are due to the singular perturbation approach in its application to a constant speed model of the T-2C airplane. Other models are of greater interest (e.g., constant thrust and variable thrust and even dynamic stall models,

Ericsson and Redding[12]) and will be treated in future research. Other techniques which complement the singular perturbation approach are also of interest. For example, the employment of optimization techniques and computational approaches that seek to satisfy necessary conditions of optimality. The singular perturbation solutions such as those obtained herein provide starting nominal state histories for such approaches. The qualitative information provided herein by the singular perturbation approach is very beneficial for future research. In practical applications, the nonchattering singular perturbation control law is probably the most useful at high pitch angles. To be explored in future research is the dominate nature of singular perturbation solutions that are part of the minimizing control laws for the full longitudinal mode (i.e. using both thrust and elevator input control).

References

[1] Lang, J.D. and Francis, M.S., "Unsteady aerodynamics and dynamic aircraft maneuverability," AGARD Symposium on "Unsteady Aerodynamics - Fundamentals and Application to Aircraft Dynamics," Gottingen, Federal Republic of Germany, 6-9 May 1985.

[2] Fossard, A.J., Modelisation et analyse des systemes a echelles de temps multiples, Ecole Nationale Superieure de l'Aeronautique et de l'Espace, Toulouse, France, 1982.

[3] Kelley, H.J., "Flight-path optimization with multiple time scales," Journal of Aircraft, Vol. 8, April 1971, 238-240.

[4] Kelley, H.J., "Aircraft maneuver optimization by reduced-order approximation," Control and Dynamic Systems, Vol. 10, edited by C.T. Leondes, Academic Press, New York, 1973, 131-178,

[5] Houlihan, S.C., E.M. Cliff and H.J. Kelley, "Study of chattering cruise," Journal of Aircraft, Vol. 19, No. 2, February 1982, 119-124.

[6] Ardema, M.D., "An introduction to singular perturbations in nonlinear optimal control," Singular Perturbations in Systems and Control, edited by M.D. Ardema, Springer Verlag, Vienna, 1982, 1-92.

[7] Ardema, M.D. and N. Rayan, "Separation of time scales in aircraft trajectory optimization," Journal of Guidance, Control and Dynamics, Vol. 8, No. 2, March-April 1985, 225-278.

[8] Shinar, J., "On applications of singular perturbation techniques in nonlinear optimal control," Automatica, Vol. 19, No. 2, 1983, 203-211.

[9] Calise, A.J., "Singular perturbation methods for variational problems in aircraft flight," IEEE Transactions on Automatic Control, Vol. AC-21, No. 3, 1976, 345-353.

[10] Stalford, H.L. and F. Garrett, Jr., "Robust nonlinear control for high angle-of-attack flight," Presented at the AIAA 25th Aerospace Sciences Meeting, Reno, Nevada, January 12-15, 1987, Paper AIAA-87-0346.

[11] Fortenbaugh, R.L., "A high angle of attack/sideslip force and moment model of the T-2C airplane," Naval Air Development Center, Warminster, PA, Internal Report, July 28, 1976.

[12] Ericsson, L.E. and J.P. Reding, "Dynamic stall at high frequency and large amplitude," J. Aircraft, Vol. 17, No. 3, 1980, 136-142.

APPENDIX A

T-2C Wind Tunnel Model for Zero Degrees Sideslip.

Table A-1a DRAG COEFFICIENT : CD WIND TUNNEL DATA (NO SIDESLIP, BETA=0)

ELEVATOR CONTROL ANGLE

ALPHA	-25	-20	-15	-10	-5	0	5	10	15
-8.	0.09830	0.09310	0.08390	0.07230	0.06335	0.05440	0.04975	0.04510	0.04470
-4.	0.04660	0.05915	0.05190	0.04300	0.03670	0.02640	0.02625	0.02610	0.02840
0.	0.04950	0.04175	0.03400	0.02790	0.02190	0.01590	0.01955	0.02280	0.02740
4.	0.04870	0.04030	0.03190	0.02760	0.02680	0.02640	0.03145	0.03650	0.04470
8.	0.06330	0.05650	0.04970	0.04408	0.04550	0.04700	0.05815	0.06930	0.07600
12.	0.09570	0.08640	0.07710	0.07580	0.08195	0.08810	0.10315	0.11820	0.12620
16.	0.12910	0.12070	0.11230	0.11380	0.12210	0.13040	0.14650	0.16260	0.17330
18.	0.14460	0.14655	0.14270	0.14270	0.16325	0.18380	0.20950	0.23520	0.25070
20.	0.20080	0.19850	0.19420	0.19380	0.20605	0.21830	0.23150	0.24470	0.25620
22.	0.25510	0.26085	0.26660	0.26900	0.27095	0.28150	0.28915	0.29680	0.30580
24.	0.30410	0.31075	0.31740	0.32150	0.32160	0.33100	0.34215	0.35330	0.36970
25.	0.44230	0.44595	0.44960	0.45370	0.46575	0.47780	0.49665	0.51510	0.51960
30.	0.54520	0.55085	0.55860	0.56740	0.58950	0.61160	0.63060	0.64960	0.65190
35.	0.66450	0.67180	0.69910	0.70340	0.70270	0.70100	0.74570	0.79040	0.80220
40.	0.80570	0.81980	0.83390	0.84970	0.86510	0.88050	0.89065	0.90080	0.95170
45.	0.91060	0.92205	0.93350	0.94500	0.95645	0.96790	0.98795	1.00800	1.02800

Table A-1b LIFT COEFFICIENT : CL WIND TUNNEL DATA (NO SIDESLIP, BETA=0)

ELEVATOR CONTROL ANGLE

ALPHA	-25	-20	-15	-10	-5	0	5	10	15
-8.	-0.7168	-0.7208	-0.7248	-0.6758	-0.6385	-0.6020	-0.5335	-0.4650	-0.4310
-4.	-0.3768	-0.3835	-0.3918	-0.3528	-0.2975	-0.2430	-0.1825	-0.1220	-0.0980
0.	0.0578	0.0688	-0.0830	0.0540	0.0760	0.1020	0.1620	0.2220	0.2450
4.	0.2760	0.2690	0.2620	0.2900	0.3595	0.4290	0.4980	0.5670	0.5850
8.	0.6000	0.6030	0.6000	0.6300	0.6950	0.7600	0.8285	0.8970	0.9120
12.	0.7170	0.9175	0.9180	0.9510	1.0160	1.0770	1.1450	1.2130	1.2190
16.	1.0280	1.0255	1.0390	1.0760	1.1365	1.1970	1.2585	1.3200	1.3240
18.	1.0490	1.0540	1.0680	1.1050	1.0985	1.0920	1.2165	1.3410	1.2960
19.	0.9140	0.9325	0.9510	0.9150	0.9610	1.0070	1.0580	1.1090	1.1170
18.	0.6890	0.7515	0.8140	0.7590	0.8315	0.9040	0.8890	0.8740	0.8810
20.	0.7240	0.7350	0.7430	0.7610	0.7915	0.8220	0.8535	0.8850	0.9130
25.	0.7850	0.8040	0.8230	0.8400	0.8770	0.9140	0.9425	0.9710	0.9720
30.	0.7590	0.7845	0.8110	0.8318	0.9425	0.9540	0.9075	0.9610	0.9760
35.	0.7820	0.8185	0.8560	0.8720	0.8870	0.8920	0.9435	0.9910	1.0000
40.	0.7930	0.8415	0.8850	0.9150	0.9160	0.9130	0.9660	1.0130	1.0240
45.	0.8240	0.8420	0.8600	0.8780	0.8960	0.9140	0.9285	0.9420	0.9578

Table A-1c PITCHING MOMENT COEFFICIENT : CM WIND TUNNEL DATA (NO SIDESLIP, BETA=0)

ELEVATOR CONTROL ANGLE

ALPHA	-25	-20	-15	-10	-5	0	5	10	15
-8.	0.4269	0.4293	0.4317	0.3518	0.2307	0.1103	-0.0101	-0.1304	-0.1994
-4.	0.3561	0.3669	0.3777	0.2946	0.1669	0.0373	-0.0870	-0.2113	-0.2757
0.	0.3045	0.3225	0.3405	0.2395	0.1032	-0.0371	-0.1641	-0.2910	-0.3633
4.	0.2537	0.2647	0.2777	0.1721	0.0324	-0.1069	-0.2341	-0.3613	-0.4159
8.	0.1965	0.2057	0.2149	0.1019	-0.0353	-0.1724	-0.3047	-0.4369	-0.4823
12.	0.1427	0.1433	0.1478	0.0339	-0.1054	-0.2427	-0.3744	-0.5060	-0.5462
16.	0.1166	0.1147	0.1126	-0.0072	-0.1450	-0.2827	-0.4106	-0.5386	-0.5752
18.	0.1044	0.0962	0.0877	-0.0267	-0.1721	-0.3155	-0.4378	-0.5600	-0.5785
19.	0.0419	0.0100	-0.0219	-0.1131	-0.2159	-0.3246	-0.4170	-0.5093	-0.5199
18.	-0.0462	-0.0949	-0.1435	-0.2017	-0.2829	-0.3623	-0.4102	-0.4581	-0.4841
20.	-0.0531	-0.0982	-0.1433	-0.2044	-0.2731	-0.3418	-0.4088	-0.4581	-0.5061
25.	-0.1328	-0.1848	-0.2365	-0.3036	-0.3736	-0.4436	-0.5025	-0.5613	-0.5797
30.	-0.1570	-0.2068	-0.2566	-0.3479	-0.4215	-0.4950	-0.5534	-0.6117	-0.6417
35.	-0.1901	-0.2612	-0.3323	-0.4055	-0.4814	-0.5573	-0.6072	-0.6570	-0.6877
40.	-0.2463	-0.3145	-0.3827	-0.4608	-0.5365	-0.6076	-0.6503	-0.6929	-0.7166
45.	-0.3188	-0.3793	-0.4398	-0.5002	-0.5607	-0.6212	-0.6584	-0.6956	-0.7328

Table A-1d

PITCH RATE DERIVATIVES : CMQ AND CZQ DATA (NO SIDESLIP, BETA=0)

ALPHA	CMQ	CZQ
-8.	-10.8227688	-6.3979818
-4.	-10.3517040	-6.5423277
0.	-10.9723968	-6.6301674
4.	-10.7597760	-6.7213897
8.	-11.0137600	-6.8328447
12.	-10.4638320	-6.8109287
16.	-10.6473680	-6.6728563
18.	-10.1809800	-6.4675160
19.	-7.4909888	-5.3747784
18.	-5.9681120	-3.7584223
20.	-4.8427328	-2.1244908
25.	-4.4010280	-2.1305711
30.	-4.8383860	-2.1322965
35.	-4.1515088	-1.8216417
40.	-3.8318920	-1.5582702
45.	-3.8988160	-1.3594094